# X-ray Diffraction studies of Aluminum Substituted Co-Mn-$FeO_4$ Nano Ferrites

M. M. Langade and D. V. Mane*

*Department of Chemistry, Shri Chhatrapati Shivaji College Omerga (M.S) - 413606*

**dvmane11@gmail.com*

**Abstract:**

Cobalt manganese aluminum ferrite systems $CoMn_{1-x}Al_xFeO_4$ has been synthesized by auto – combustion method from corresponding metal nitrates. X-Ray diffraction pattern indicate well defined peaks of crystalline F.C.C. phase which confirms spinel cubic structure formation. The lattice parameters are found to be decrease with increasing $Al^{3+}$ substitution. X-Ray density of all sample decrease with $Al^{3+}$ substitution due to influence of atomic weight.

.

## 1 Introduction

Magnetic nanoparticles attention recently due to their technological applications in microwave devices, high-density magnetic recording, electronic devices and medical instruments [1-4]. The spinel ferrites magnetic nanoparticles are technologically important due to their various applications and the interesting physics and chemistry involved in. The recent trend is focused on the doped ferrites prepared using various synthesis techniques with different cation concentrations which affects the various properties like, electrical, dielectric, and magnetic behavior. [5-8]

Ferrite materials are important magnetic materials, which have various applications in power conditioning and conversion. Due to their distinct magnetic properties, ferrite materials have been widely used to prepare many electromagnetic devices such as inductors, converters, phase shifters and electromagnetic wave absorbers [9,10]

Since, the temperature dependence of the magnetoelastic properties is strongly dependent on the magnetostriction and magnetic anisotropy, as well as coercivity, permeability, and chemical composition of the material. As per the literature review these properties appeared excellent with Co-Mn ferrite, therefore in our present study we have kept Co-$MnFeO_4$ as a basic composition for further investigation.

A variety of techniques have been used to prepare ferrite materials of nano-scale including co-precipitation method [11-15], sol–gel process [16-18], glass crystallization [19], the mechanical alloying method [20] self-propagation microemulsion, microwave, hydrothermal, and ultrasound-assisted synthesis.

Keeping the importance of Co-Mn ferrite and the need to prepared these samples in nanometer dimensions it was decided to synthesize $CoMn_{1-x}Al_xFeO_4$ (x = 0.0, 0.25, 0.5, 0.75, 1.0) ferrite system. The structural and magnetic changes in the Co-Mn ferrite brought by the $Al^{3+}$ substitution synthesized via sol-gel auto-combustion method is discussed here.

## 2 Experimental

Sol-gel auto-combustion route was adopted to achieve the homogeneous mixing of the chemical constituents at the atomic scale and better sinterability. AR grade cobalt nitrate ($Co(NO_3)_2 \cdot 3H_2O$), aluminum nitrate ($Al(NO_3)_3 \cdot 9H_2O$), manganese nitrate ($Mn(NO_3)_2 \cdot 6H_2O$),iron nitrate ($Fe(NO_3)_3 \cdot 9H_2O$) and citric acid ($C_6H_8O_7 \cdot H_2O$),were used to prepare the $CoMn_{1-x}Al_xFeO_4$ (x = 0.0, 0.25, 0.5, 0.75, 1.0) ferrite compositions. Reaction procedure was carried out in air atmosphere without protection of inert gases. The molar ratio of metal nitrates to citric acid was taken as 1:3. The metal nitrates were dissolved together in a minimum amount of double distilled water to get a clear solution. An aqueous solution of citric acid was mixed with metal nitrates solution, then ammonia solution was slowly added to adjust the pH at 7. Then the solution was heated to 90 ºC to transform it into gel. When ignited at any point of the gel, the dried gel burnt in a self-propagating combustion manner until all gels were completely burnt out to form a fluffy loose powder. The auto-combustion was completed within a minute, yielding the brown-colored ashes termed as a precursor. Finally, the as prepared ferrite powder was annealed at 600 ºC for 4 h. in order to compete the crystallization.

The crystal structure of prepared samples was characterized by X-ray diffraction technique using Phillips X-ray diffractometer (Model 3710) equipped with Cu-$K_\alpha$ radiation (λ=1.5405Å). The microstructure was examined on the fracture surfaces of the samples using thermal field emission scanning electron microscope (SEM). Transmission electron microscope (TEM) measurements were recorded on Philips (Model CM 200). The samples were prepared by dispersing the powders in acetone and dropping the suspension on a lacey carbon film supported on a 300-mesh copper grid. The infrared spectra of all the samples were recorded at room temperature in the range 300 $cm^{-1}$ to 800 $cm^{-1}$ using Perkin Elmer infrared spectrophotometer. Room temperature magnetization of the samples was measured using the pulse field magnetization set-up.

## 3 Results and discussion

### 3.1 Structural Analysis

Prepared samples were tested by X-ray diffraction. Fig. 1.shows the XRD patterns of the samples with different doping levels of $Al^{3+}$ substitution.

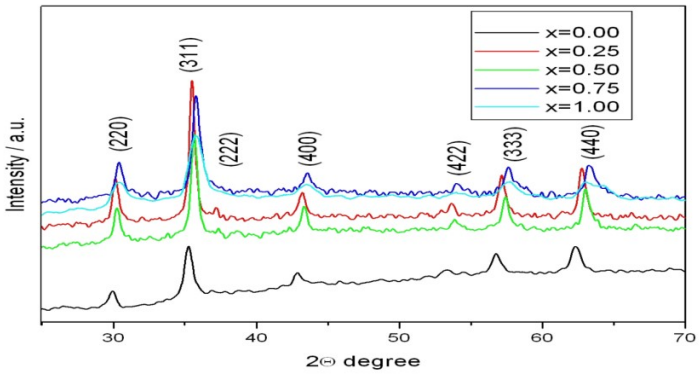


**Fig. 1** X-ray diffraction pattern of $CoMn_{1-x}Al_xFeO_4$ (x= 0.00,0.25,0.50,0.75,1.00)

The reflection from the planes, (2 2 0), (3 1 1), (2 2 2), (4 0 0), (4 2 2), (333) and (4 4 0) appeared for all samples. The patterns indicate well-defined peaks of crystalline FCC phase which confirm spinel cubic structure

formation for the samples and belong to the ($Fd^3m$) cubic spinel space group. The lattice parameters have been computed using the d-spacing values and the respective (h k l) parameters from the classical formula given in Eq.1

$$a = \frac{\lambda}{2}\frac{\sqrt{(h^2 + k^2 + l^2)}}{\sin\theta} \qquad \ldots\ldots \qquad \textbf{(1)}$$

Where *d* is the inter-planer spacing and (*hkl*) is the index of the XRD reflection peak. The lattice constant is affected by the cationic stoichiometry. The lattice parameters are found to decrease almost linearly by increasing $Al^{3+}$ substitution. The values of the lattice parameter exhibit an almost linear dependence, thus obeying Vegard's law [32]as shown in Table.1.

| Comp. x | a (Å) | dx ($g/cm^3$) | $D_{XRD}$ (nm) | $d_B$ ($g/cm^3$) | P (%) |
|---|---|---|---|---|---|
| 0.00 | 8.394 | 5.249 | 16.028 | 4.121 | 21.50 |
| 0.25 | 8.349 | 5.175 | 18.132 | 4.050 | 21.74 |
| 0.50 | 8.339 | 5.034 | 9.482 | 3.923 | 22.07 |
| 0.75 | 8.321 | 4.905 | 12.276 | 3.818 | 22.17 |
| 1.00 | 8.214 | 4.932 | 9.070 | 3.782 | 23.32 |

**Table .1.** Lattice constant (a), X-ray density ($d_x$), crystallite size ($D_{XRD}$), bulk density ($d_B$) and porosity (P)

The X-ray density (dx) of all the samples of the series was obtained by the following relation:

$$dx = \frac{8M}{Na^3} \qquad \ldots\ldots.. \qquad \textbf{(2)}$$

where '8' is the number of molecules per unit cell, 'M' is the molecular weight of sample, 'N' is the Avogadro's number and 'a' is lattice constant. It can be observed from Table 1, the value of $d_x$ decreases with $Al^{3+}$ substitution. This may be due to the fact that the density and atomic weight of $Al^{3+}$ are smaller than that of $Mn^{3+}$ ions. The density and atomic weight of $Al^{3+}$ is 2.70 $g\cdot cm^{-3}$ and 26.98 respectively whereas it is 7.23 $g\cdot cm^{-3}$ and 54.93 respectively for $Mn^{3+}$ ion.

However, the bulk density ($d_B$) calculated from the Archimedes principle depicted in Table.1,shows the smaller value as compared to that of dx. The smaller value of $d_B$ than that of the $d_x$ is due to the existence of pores that depend on the sintering and pressing conditions. The peaks of (2 2 0), (3 1 1), (2 2 2), (4 0 0), (4 2 2), (333) and (4 4 0) have been deconvoluted to Lorentzian curves for the determination of the crystallite size using full-width at half maximum value. The crystallite size of the nanocrystalline samples were measured from XRD line broadening analysis applying Scherrer's formula :

$$D_{XRD} = \frac{k\lambda}{\beta\cos\theta} \qquad \ldots\ldots\ldots \qquad \textbf{(3)}$$

Where $D_{XRD}$ is the dimension of the crystallites, λ the wavelength of the X-ray radiation, θ the Bragg angle, k is a shape factor taken to be 0.94 and β the peak width measured at half of the maximum intensity. The values are presented in Table 1.The values of the $D_{XRD}$ are in the range of 18 to 9 nm and showed reasonable decreasing trend with the increase in $Al^{3+}$ substitution in Co-Mn ferrite.

The percentage porosity (P) is calculated using the following relation:

$$P = \left( \frac{d_X - d_B}{d_X} \right) \times 100 \quad \text{……..} \qquad \textbf{(4)}$$

Where dx and $d_B$ are the X-ray density and bulk density respectively. Table 1. shows that the porosity of the samples increases with $Al^{3+}$ substitution; this maybe due to the release of oxygen from the samples during sintering i.e., the decrease in oxygen ion(anion) diffusion would retard the densification. The increase in porosity with $Al^{3+}$ substitution is also related to the decrease in bulk density and decrease in crystallite size.

$L_A$ and $L_B$ i.e. the hopping length for tetrahedral A- and octahedral B-sites respectively were calculated using the following relation:

$$L_A = a\sqrt{\frac{3}{4}} \quad \text{…….} \qquad \textbf{(5)}$$

$$L_B = a\sqrt{\frac{2}{4}} \quad \text{…….} \qquad \textbf{(6)}$$

The variation of hopping lengths $L_A$ and $L_B$ with $Al^{3+}$substitution is depicted in Fig. 2 It is observed from Fig. 2 that the distance between the magnetic ions (hopping length) decreased with $Al^{3+}$ substitution.

| Comp. x | Hopping length | | $d_{AX}$ (Å) | $d_{BX}$ (Å) | Tetra edge (Å) | Octa edge $d_{BXE}$ (Å) | |
|---|---|---|---|---|---|---|---|
| | $L_A$ (Å) | $L_B$ (Å) | | | $d_{AXE}$ | Shared | unshared |
| 0.00 | 3.6347 | 2.9677 | 1.905 | 2.052 | 3.110 | 2.825 | 2.975 |
| 0.25 | 3.6152 | 2.9518 | 1.894 | 2.041 | 3.093 | 2.810 | 2.959 |
| 0.50 | 3.6109 | 2.9483 | 1.892 | 2.038 | 3.089 | 2.806 | 2.956 |
| 0.75 | 3.6031 | 2.9419 | 1.888 | 2.034 | 3.083 | 2.800 | 2.949 |
| 1.00 | 3.5568 | 2.9041 | 1.864 | 2.008 | 3.043 | 2.764 | 2.912 |

**Table.2**. Hopping lengths ($L_A$ and $L_B$), Tetrahedral bond ($d_{AX}$), octahedral bond ($d_{BX}$), tetra edge ($d_{AXE}$) and octahedral edge ($d_{BXE}$) (shared and unshared) of $CoMn_{1-x}Al_xFeO_4$

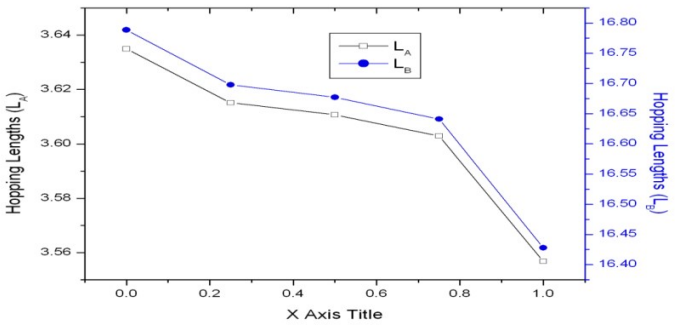


**Fig. 2** Hopping length $L_A$ and $L_B$

This behavior of hopping lengths with $Al^{3+}$ substitution is in agreement with the variation in lattice constant with $Al^{3+}$ substitution. The variation of $L_A$ and $L_B$ may be related to the difference in the ionic radii between $Al^{3+}$ and $Mn^{3+}$ ions. The substitution of $Al^{3+}$ ions instead of $Mn^{3+}$ ions makes the magnetic ions become smaller to each other and the hopping length decreased.

## 4 Conclusions

$Al^{3+}$substitutedCo-Mn ferrites nanoparticles with a chemical formula $CoMn_{1-x}Al_xFeO_4$ where x = 0.0, 0.25, 0.5, 0.75, 1.0 were synthesized via the sol-gel auto-combustion method. Co-Mn ferrites nanoparticles synthesized by sol-gel auto-combustion method has been characterized to be single phased cubic spinel belonging to the space group Fd 3m.The lattice constant of Co-Mn ferrite decreased linearly with the increase of $Al^{3+}$substitution and may be related to the smaller ionic radii of $Al^{3+}$ ions as compared to that of $Mn^{3+}$ ions.

**Acknowledgement**

The authors are very much thankful to Head of the Chemistry Dept and Principal, Shri Chhatrapati Shivaji College , Omerga for providing necessary facilities and cooperation during the course of work.

## References

1. M.H. Sousa, F.A. Tourinho, J. Depeyrot, G.J. da Silva, M.C.F.L. Lara, J. Phys. Chem.B 105 (2001) 1168–1175.
2. Sagar E. Shirsath, Mahesh L. Mane, Yukiko Yasukawa, Xiaoxi Liu and Akimitsu Morisako, Phys. Chem. Chem. Phys. 16 (2014) 2347-2357.
3. Ali Ghasemi, Sagar E. Shirsath, Xiaoxi Liu, and Akimitsu Morisako, J. Appl. Phys. 109 (2011) 07A507
4. Y.F. Lu, W.D. Song, Appl. Phys. Lett. 76 (2000) 490–492.
5. A. Baykal, N. Kasapogul, Y. Koseoglu, A.C. Basaran, H. Kavas, M.S. Toprak, Cent.Eur. J. Chem. 6 (1) (2008) 125–130.

6. C. Venkataraju, G. Sathishkumar, K. Sivakumar, J. Magn. Magn.Mater. 322(2010) 230–233.
7. Sagar E. Shirsath, Yukiko Yasukawa, Ali Ghasemi, Xiaoxi Liu, and Akimitsu Morisako, J. Appl. Phys. 115 (2014) 17A515.
8. M.R. Bhandare, H.V. Jamadar, A.T. Pathan, B.K. Chougule, A.M. Shaikh, J. Alloys Compd.509 (2011) L113–L118.
9. Alex Goldman, Modern Ferrite Technology, 2nd ed. (Springer, New York, 2006).
10. Zhijian Peng, XiuliFu, HuilinGe, ZhiqiangFu, ChengbiaoWang, LonghaoQi, HezhuoMiao, Effect of$Pr^{3+}$doping onmagneticanddielectricproperties of Ni–Znferritesby‘‘one-stepsynthesis’’ J.Magn.Magn.Mater. 323 (2011) 2513–2518
11. D.H. Chen, Y.Y. Chen, Mater. Res. Bull. 37 (2002) 801–810.
12. S. M. Patange, Sagar E. Shirsath, G. S. Jangam, K. S. Lohar, S. S. Jadhav, K. M. Jadhav, J. Appl. Phys. 109 (2011) 053909
13. V. Uskokovi´ c1, D. Makovec, M. Drofenik, Mater. Sci. Forum 494 (2005) 155–160.
14. Z.F. Zi, Y.P. Sun, X.B. Zhu, Z.R. Yang, J.M. dai, W.H. Song, J. Magn. Magn.Mater.320 (2008) 2746–2751.
15. M.M. Hessien, M.M. Rashad, K. El-Barawy, J. Magn. Magn.Mater. 320 (2008)336–343.
16. Sagar E. Shirsath, R. H. Kadam, S. M. Patange, M. L. Mane, Ali Ghasemi, Akimitsu Morisako, Appl. Phys.Lett.100 (2012) 042407.
17. Y. Wang, Q. Li, C. Zhang, H. Jing, J. Alloys Compd. 467 (2009) 284–287.
18. Y. Wang, Q. Li, C. Zhang, B. Li, J. Magn. Magn.Mater. 321 (2009) 3368–3372.
19. H. Sato, T. Umeda, J. Mater. Trans. 34 (1993) 76–81.
20. J. Ding, W.F. Miao, P.G. McCormick, R. Street, J. Alloys Compd. 281 (1998) 32–36.

- ***Paper is submitted for poster presentation at Pre Science Congress 2014 , 30 &31 st December, 2014 at DR. B.A.M. University, Aurangabad***